Journal of Zhejiang University-SCIENCE A (Applied Physics & Engineering)
ISSN 1673-565X (Print); ISSN 1862-1775 (Online)
www.zju.edu.cn/jzus; www.springerlink.com
E-mail: jzus@zju.edu.cn

Parametric formulae for axial stiffness of CHS X-joints subjected to brace axial tension

Guo-zhi QIU†, Jing-hai GONG, Jin-cheng ZHAO

(*Department of Civil Engineering, Shanghai Jiao Tong University, Shanghai 200240, China*)

†E-mail: qiugz@sjtu.edu.cn

Received Jan. 17, 2010; Revision accepted July 9, 2010; Crosschecked Jan. 7, 2011

Abstract: Recent research has shown that circular hollow section (CHS) joints may exhibit non-rigid behavior under axial load or bending. The non-rigid behavior significantly affects the mechanical performance of structures. This paper is concerned with the parametric formulae for predicting axial stiffness of CHS X-joints while braces are in tension. The factors influencing the axial stiffness of CHS X-joints under brace axial tension are investigated, including the joint geometric parameters, the axial force of the chord, and bending moments of braces in two directions, etc. Effects of various parameters on axial stiffness of CHS X-joints are examined by systematic single-parameter nonlinear analysis using shell finite element methods. The analysis is implemented in a finite element code, ANSYS. The observed trends form the basis of the formulae for calculating the joint axial stiffness under brace axial tension by multivariate regression technique. In order to simplify the formulae, two non-dimensional variables are introduced. The proposed formulae can be used to calculate the joint axial stiffness in the design of single-layer steel tubular structures.

Key words: Joint stiffness, Brace tension, Parametric analysis, Stiffness formula
doi:10.1631/jzus.A1000022 **Document code:** A **CLC number:** TU392

1 Introduction

Circular hollow section (CHS) tubular joints are widely used in space structures. A great effort has been made to investigate the strength of tubular joints (Soh *et al*., 2000; Choo *et al*., 2003; 2006; Shu *et al*., 2004; Qian *et al*., 2005; Gho *et al*., 2006; Schumacher *et al*., 2009). CHS tubular joints are usually assumed to be pinned or rigid. It has been shown that tubular joints may exhibit non-rigid behavior under axial load or bending (Chen *et al*., 2001; Wang, 2005). The non-rigid behavior affects the mechanical performance of structures significantly (Yang *et al*., 1990; Chen and Zhang, 1996; Wang and Chen, 2005; Lopez *et al*., 2007; Ihaddoudenea *et al*., 2009; Turker *et al*., 2009). Wang (2005) established parametric formulae for predicting rigidities or flexibilities of tubular joints on the basis of finite element (FE) analyses on nine T(Y) type and 25 K type joint models, but the internal forces of tubular joint members were not considered. In order to perform optimal designs of both the safety and economy of tubular structures, it is necessary to study their non-rigidity behaviors.

Based on a single-layer spherical shell project, extensive work on the non-rigidity characteristics of CHS X-joints has been done by Qiu and Zhao (2008; 2009; 2010). An experimental study of six CHS X-joint specimens was carried out with the braces subjected to axial force, out-of-plane moment, and in-plane moment (Qiu and Zhao, 2008). The mechanical behaviors and failure modes of the joints were obtained. The joint specimens were analyzed by nonlinear finite element methods. The systematic single-parameter nonlinear analysis of the related factors was then carried out. New formulae for axial stiffness of CHS X-joints under brace axial compression (Qiu and Zhao, 2009) and tension, bending stiffness under out-of-plane, and in-plane moments of braces were

proposed using multivariate regression technique. The influence of joint non-rigidity on the global performance of tubular structures was investigated (Qiu and Zhao, 2010). In this paper, studies on joint axial stiffness under brace axial tension are undertaken.

2 Two non-dimensional variables

In order to simplify the formulae for joint axial stiffness and speed up the multiple regression analysis, two non-dimensional variables, joint axial load capacity factor ω_N and joint axial stiffness factor η_N, are introduced (Qiu and Zhao, 2009). Parameter ω_N is obtained as follows:

$$\omega_N = \frac{N}{N_{tX}^{pj}}, \tag{1}$$

where N is the axial load applied on the braces, and N_{tX}^{pj} is the maximum allowable tensile force applied on the braces, which is given in the current Chinese steel design code (GB 50017-2003). Although ω_N usually ranges from 0.3 to 1.0 in actual tubular structures, it may be greater than 1.0 when analyzing the stability of single-layer tubular structures.

Parameter η_N is defined by

$$\eta_N = \frac{K_N}{EA / L_{100}}, \tag{2}$$

where K_N is the axial stiffness of CHS X-joints, E is the elastic modulus, and A is the cross section area of the brace. L_{100}=100×r, where r is the least radius of gyration of the brace. EA/L_{100} is the axial stiffness of the braces with a slenderness ratio of 100, and taken as the reference value in this study.

It can be found from the definition that the two variables vary over a small range. Thus, the computational formulae of axial stiffness of CHS X-joints can be easily derived using the multivariate regression method.

3 Numerical models

A FE code, ANSYS (SAS, 2002) was used for the numerical analysis. The midsurfaces of the joint member walls were modeled using the mesh of 4-node elastic-plastic shell elements (SHELL181). A fine mesh was created in the vicinity of the joint intersection. A mesh sensitivity study, varying the mesh density at joint intersections, was conducted to obtain a suitable mesh size for modeling the joint prior to the extensive FE analysis. Boundary conditions are shown in Fig. 1, where one end of the chord was pinned, while the other end of the chord was a two direction hinge, which means only displacements along the axis are allowed. The load was applied uniformly on the cross section at the free ends of the braces. A typical FE mesh of a CHS X-joint under brace axial tension is shown in Fig. 1. The mechanical properties of Q235 steel, which is broadly used in China's construction industry, were adopted in the simulation. The yield strength of Q235 steel is f_y=235 MPa. The nonlinear material properties were taken into account by assuming the stress-strain relationship as a bilinear curve with E=2.06×10^5 MPa, and the plastic modulus being 2.06×10^3 MPa (Choo *et al.*, 2003). According to Wang (2005), the weld effect on the joint elastic stiffness can be ignored, and therefore the weld was not modeled in the FE analysis.

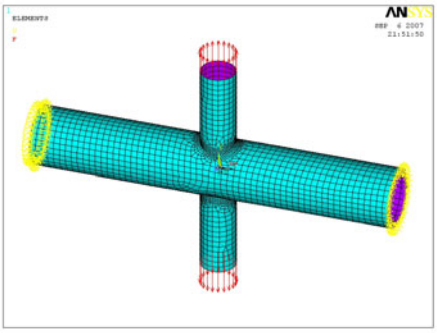

Fig. 1 Finite element model of a tubular X-joint

4 Verification study

In order to investigate the axial rigidity of CHS X-joints and validate the numerical analysis model, experiments on CHS X-joint rigidity were carried out (Qiu and Zhao, 2008). The chord of the specimen was Φ351 mm×8 mm, the braces were Φ351 mm×8 mm and Φ219 mm×6 mm, and the steel material was Q345. The load applying device is shown in Fig. 2.

As shown in Fig. 3, the joint failure mode is buckling of the chord wall. The deformation of the

chord wall connected with the brace Φ219 mm×6 mm is large, while that of the end of the branch Φ351 mm×8 mm is very small. This indicates that when the parameter β is smaller, the joint axial stiffness is weaker.

Fig. 2 Load applying device

Fig. 3 Failure mode of the specimen

The FE analysis of the specimen was carried out using ANYSYS. The joint deformation of FE results when the load is close to the ultimate load, is shown in Fig. 4. When the axial force of the brace increases to a certain value, extensive yielding in the chord wall appears at the intersection region with the smaller brace. It can be observed from Figs. 3 and 4 that the joint deformation is similar. Relationship curves between the axial load N of the Φ219 mm×6 mm brace and the joint deformation δ are shown in Fig. 5. Through comparisons between the FE predictions and experimental results, good agreement was observed.

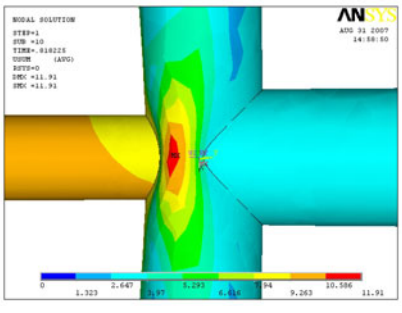

Fig. 4 Deformation mode of the finite element model (mm)

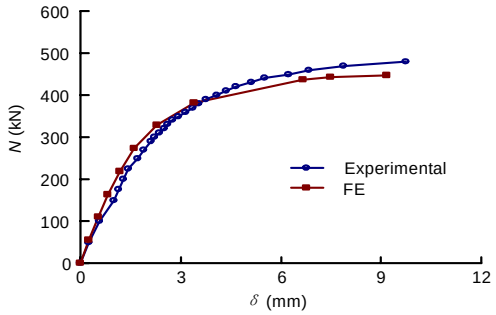

Fig. 5 Axial load-deformation curves

5 Parametric studies

In this parametric study, 66 FE models of CHS X-joints were created to evaluate the effects of different factors on the joint stiffness under brace axial tension. The influence factors of joint stiffness can be classified into two categories. One category is related to joint geometric parameters, as illustrated in Fig. 6, which include β, γ, τ, θ, and β_2. When the chord diameter D and the relevant parameters are given, the joint geometry is specified. For each geometric parameter, the range commonly used in the industry was covered. The other category is in relation to the

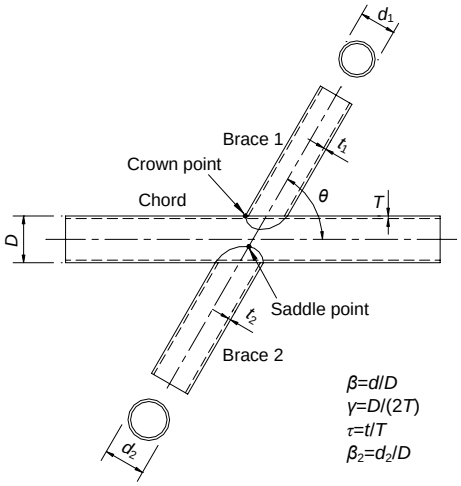

Fig. 6 Geometrical parameters of a tubular X-joint
D: diameter of the chord; d_1, d_2: diameters of the braces; T: wall thickness of the chord; t_1, t_2: wall thicknesses of the braces; θ: brace inclination angle

internal force of chord and braces, such as σ/f_y (σ is the chord stress, and f_y is the steel yield strength), M_I (in-plane moment), M_W (out-of-plane moment), etc.

In a single-parameter analysis, one parameter is changed from one analysis to the next, while others are kept constant. The variations of joint axial stiffness are only affected by this single parameter, and therefore the effects of the parameter can be determined.

5.1 Effect of parameter β

Parameter β varies from 0.2 to 1.0, with an increment of 0.1. The size of the chord member is Φ500 mm×16 mm, the wall thickness of the two symmetrical braces is 8 mm, and the diameters of the two braces can be obtained by the β value. The inclination angle of the braces is fixed at 90°. Chord stress and brace moments are not considered.

As shown in Fig. 7, the trends of the curves for different β values are similar. The axial stiffness of the joints increases slightly when the load level is very small, and then decreases with the increase of axial load on the braces. It is different with the trends of the curves when the joints are subjected to brace axial compression (Qiu and Zhao, 2009). A possible reason is that the initial brace tension causes compressive stress at the outer side of the chord wall, which constrains the deformation of the joint. A progressive increase in the joint initial axial stiffness with an increase in β value can also be observed. When ω_N<0.4, the joint axial stiffness varies marginally for a certain β. However, when ω_N>0.4, the joint axial stiffness decreases rapidly and η_N is even less than 0.5 for β<0.5 and $\omega_N\geq$1.0. It is worth mentioning that even for joints with very high initial axial stiffness, i.e., β>0.9, η_N is less than 1 when the brace tension reaches the joint load capacity ($\omega_N\geq$1.0). Therefore, the axial stiffness of CHS X-joints under brace tension has a significant effect on tubular structures, and must be considered in the practical design.

5.2 Effect of parameter γ

Considering the possible member size in the actual design, parameter γ of the joints varies from 10 to 50, with an increment of 5. The diameter of the chord is 600 mm, and the diameter of the two symmetrical braces is 300 mm. Parameter τ is fixed at 0.5. The thickness of chord wall and brace wall can be evaluated by the γ value and τ value. The inclination angle of the braces is 90°. Chord stress and brace moments are not considered.

Relationship curves between η_N and ω_N of the joints for different γ are shown in Fig. 8. All the curves tend to be "converging" for high ω_N values. For joints with $10\leq\gamma\leq20$, when ω_N<0.5, η_N is greater than or close to 1.0, which means the joint axial stiffness is greater than or close to the axial stiffness of the brace members. When $\omega_N\geq$0.5, η_N value drops rapidly with the increase of ω_N. It can be observed that for joints with high γ values (γ>20), η_N is less than 0.7 even when ω_N<0.5. This indicates that the γ value of CHS X-joints needs to be less than 20.

5.3 Effect of parameter τ

The thickness of the brace wall is normally less than the thickness of the chord wall. Thus, the X-joints with τ=0.2–1.0, with an increment of 0.1, are analyzed in this study. The size of joint chord member is Φ500 mm×20 mm, and the diameter of the two symmetrical braces is 300 mm. The thickness of the brace wall is evaluated by the τ value. The inclination angle of the brace is 90°. Chord stress and brace moments are not considered.

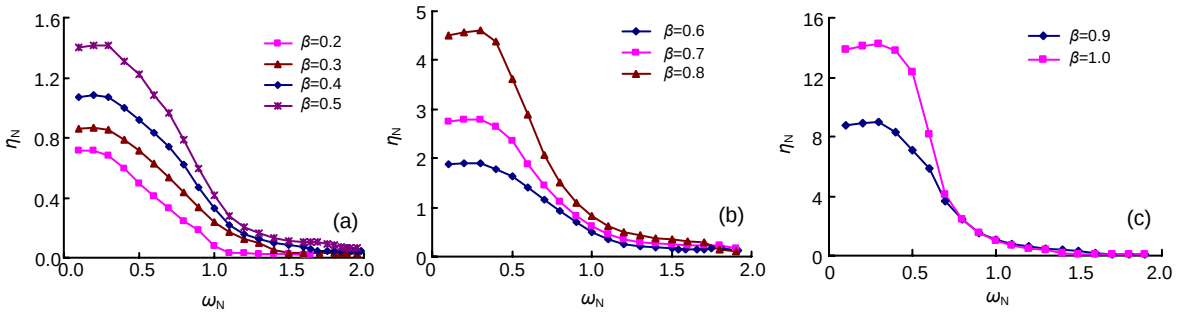

Fig. 7 Comparison of the joints subjected to brace tension with different β
(a) β=0.2, 0.3, 0.4, 0.5; (b) β=0.6, 0.7, 0.8; (c) β=0.9, 1.0

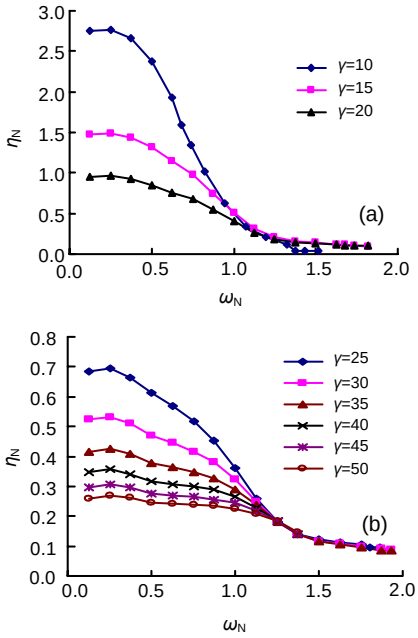

Fig. 8 Comparison of the joints with different γ
(a) γ=10, 15, 20; (b) γ=25, 30, 35, 40, 45, 50

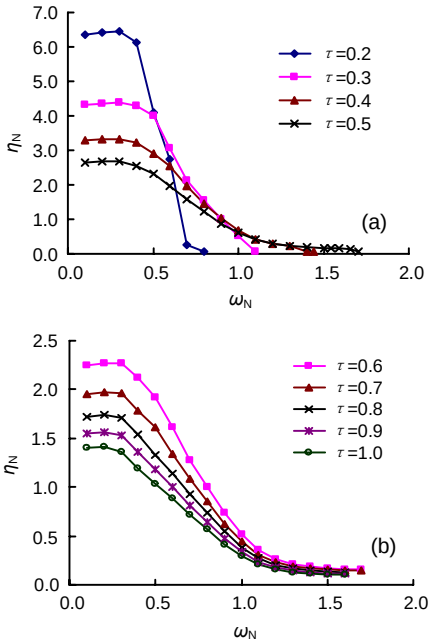

Fig. 9 Comparison of the joints with different τ
(a) τ=0.2, 0.3, 0.4, 0.5; (b) τ=0.6, 0.7, 0.8, 0.9, 1.0

Fig. 9 presents the η_N-ω_N curves for X-joints with different τ. For X-joints with low τ values ($\tau \leq 0.5$), η_N values are all greater than 2.5 when $\omega_N \leq 0.4$. For joints with high τ values ($\tau > 0.5$), however, η_N values are all less than 2.3. This indicates that the X-joints stiffness under brace axial tension must be considered in the practical design. But it should be noted that the parameter τ has little influence on the X-joints stiffness. According to the definition of η_N, the variation of η_N with different τ is mainly caused by the change of the axial stiffness of the braces with different wall thickness.

5.4 Effect of brace inclination angle θ

The intersection line between the brace and the chord varies with changes in the brace inclination angle θ. For joints with θ=90°, the stresses of the two crown points of the brace are identical. For joints with low θ values, e.g., θ=30°, the stress of the crown points closer to the saddle points is higher.

In the current study, the inclination angle θ of the brace varies from 30° to 90°, with an increment of 10°. The size of the chord member is Φ500 mm ×20 mm, and those of the two braces are Φ300 mm ×12 mm. Brace moments and chord stress are not considered.

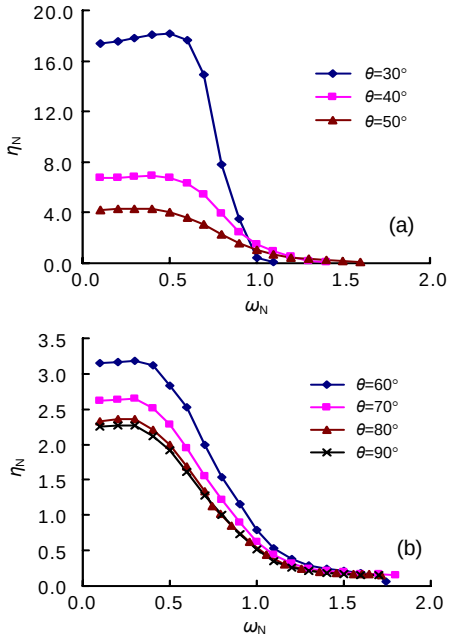

Fig. 10 Comparison of the joints with different θ
(a) θ=30°, 40°, 50°; (b) θ=60°, 70°, 80°, 90°

As shown in Fig. 10, the load transfer paths in the joints change with different inclination angles of the brace. There is a progressive reduction in the axial stiffness of X-joints with the increase of θ value. Parameter η_N nearly remains constant when ω_N is low,

but it decreases rapidly after ω_N exceeds a certain value.

5.5 Effect of the chord stress ratio

The chord stress ratio σ/f_y ranges from −0.91 to 0.91. When $\sigma/f_y=\pm0.91$, $\sigma=\pm f$ (f=215 MPa, design strength of Q235 steel). The negative sign indicates that the stress applied to the chord is compressive. The size of the chord member is Φ500 mm×20 mm, and those of the two symmetrical braces are Φ300 mm×12 mm. The brace inclination angle is 90°. Brace moments are not considered. Chord stresses are applied as a uniform pressure on the cross section at the end of the chord member. The chord is pre-loaded and the load level is maintained throughout the analysis, while the brace axial force is loaded incrementally.

As shown in Fig. 11a, the axial stiffness of the joints decreases with the increase of compressive chord stress at the beginning of loading, during which the braces are under tension and the chord is under compression. This is more obvious in joints with a high chord compressive stress. The reason is that the brace tension causes compressive stress at the outer side of the chord walls between the saddle points. When the chord is pre-loaded compressively, it increases the deformation of the chord walls, and therefore the initial axial stiffness of joints is decreased. After part of the chord walls yield, the influence is gone. There is a marginal difference between the curves when $-0.6\leq\sigma/f_y\leq0$. However, when $-0.91\leq\sigma/f_y\leq-0.8$, η_N clearly decreases.

As shown in Fig. 11b, the axial stiffness of the joints is enhanced by the tensile chord stress at the initial period of loading. The reason is that the chord tensile stress constrains the deformation of the chord walls when the joints are subjected to brace tension. Note that the axial stiffness of the joints decreases with increases in brace tension, and the curves converge to the level of initial stiffness for $\sigma/f_y=0$. This is more obvious in the joints with high chord stress levels (large σ/f_y values).

5.6 Effect of bending moments of braces

The bending moments of the braces include the in-plane moment M_I and the out-of-plane moment M_W. σ_I/f and σ_W/f ($\sigma_I=M_I/W$, $\sigma_W=M_W/W$, where W is the section modulus, and f is the steel design strength of braces) are used as influence parameters to analyze the joint stiffness under brace axial tension. Six stress levels, 0, 0.2, 0.4, 0.6, 0.8, and 1.0, are considered. The FE models are the same as that for analyzing the effect of the chord stress ratio, but the chord stress is not considered. The brace moment is pre-loaded and maintains constant, and then the brace axial tension is incrementally applied.

The comparison of η_N-ω_N relationship curves for different σ_I/f is shown in Fig. 12. The joint axial stiffness is enhanced at the beginning of the tensile loading on braces. It is more obvious for joints subjected to large in-plane moments, but it drops rapidly with increases in brace tensile loading. Note that the

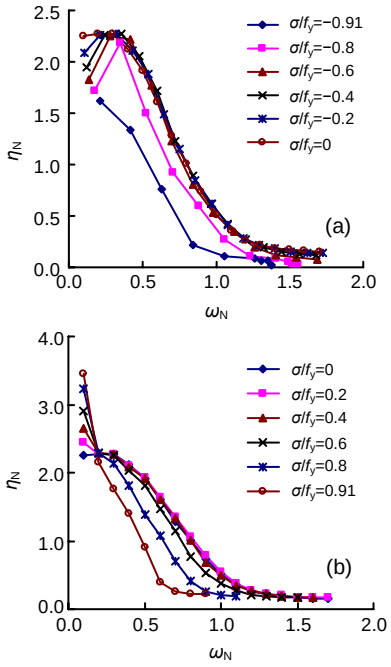

Fig. 11 Comparison of the joints with compressive chord stress (a) and tensile chord stress (b)

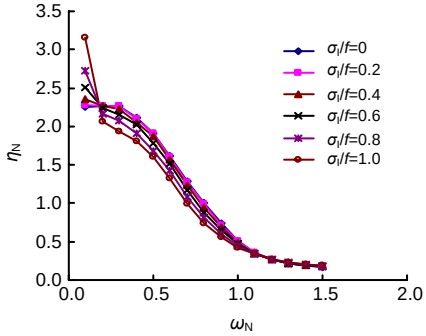

Fig. 12 Effect of in-plane moment

effect of the in-plane moment on the axial stiffness of X-joints subjected to brace tension is not significant, and can be ignored in the practical design.

Fig. 13 presents the η_N-ω_N curves of the joints with different σ_W/f. The initial axial stiffness of the joint with σ_W/f=1.0 is about half of that with σ_W/f=0. The effect of the out-of-plane moment on the axial stiffness of the X-joints subjected to brace tension is obvious.

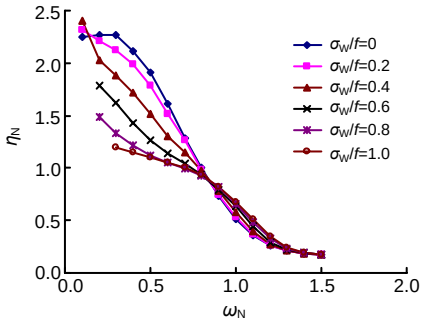

Fig. 13 Effect of out-of-plane moment

5.7 Effect of the diameter of the other brace

To investigate the effect of the interaction between the two braces on the axial stiffness of X-joints, the joint axial stiffness of one brace (labeled Brace 1 with diameter d_1) is analyzed with consideration of the diameter of the other brace (labeled Brace 2 with diameter d_2). The size of the chord member is Φ500 mm×20 mm, the brace wall thickness is 10 mm, and the brace inclination angle is 90°. Brace moments and chord stress are ignored. Three groups of models, whose diameter ratios (β) of Brace 1 to the chord are 0.3, 0.6, and 0.9, are analyzed.

K_N-ω_N curves for the three groups of models are shown in Fig. 14. When the diameter of Brace 1 d_1 is unchanged, the axial stiffness increases with the increase of d_2. It is even more obvious for the joints with large diameter of Brace 1; e.g., when d_1=450 mm, the initial joint axial stiffness for d_2=450 mm is about 2.5 times of that for d_2=150 mm. Thus, the effect of the other brace on the joint stiffness needs to be considered in the design.

6 Axial stiffness formulae of CHS X-joints under brace tension

The influence of each parameter has been studied through single-parameter analysis in the previous section. Meanwhile, the formulae for calculating the axial stiffness of X-joints are functions of axial loading in the braces. A regression analysis on the present results is carried out to derive formulae for the joint axial stiffness under brace tension (Gho and Yang, 2008).

Parameter ω_N and the geometric parameters need to be analyzed separately. The relationship between the two parameters, η_N and ω_N, is first determined, and then the X-joint axial stiffness value is computed accordingly.

According to the common feature of the η_N-ω_N curves, which were obtained in the previous analysis, the η_N-ω_N relationship is discretized into two types of curves, as shown in Fig. 15 (Qiu and Zhao, 2009).

After the discretization of the η_N-ω_N relationship, the curves can be determined by the four control points *A*, *B*, *C*, and *D*. In this way, the regression of η_N is equivalent to those of η_{N0}, ω_{N95}, ω_{N50}, and ω_{N10}, where η_{N0} is the initial joint axial stiffness factor, and ω_{N95}, ω_{N50}, and ω_{N10} are the ω values corresponding to η_N values equal to 0.95η_N, 0.5η_N, 0.1η_N, respectively.

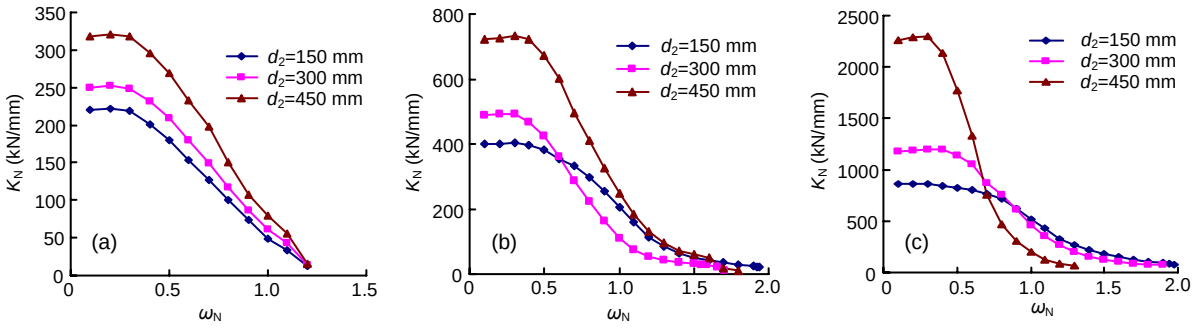

Fig. 14 Effect of the diameter of the other brace
(a) d_1=150 mm; (b) d_1=300 mm; (c) d_1=450 mm

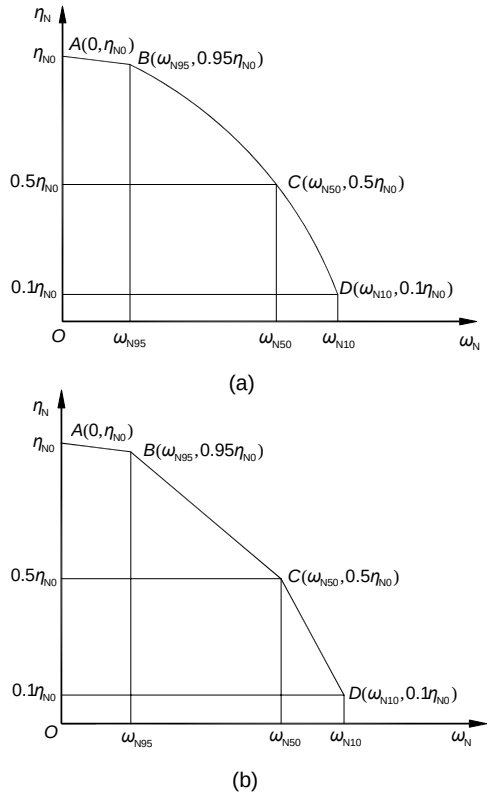

Fig. 15 Two types of relationship curves
(a) *BCD* is a quadratic curve; (b) *BCD* is a bilinear curve (Qiu and Zhao, 2009)

Before applying loads on the tubular structures, the internal forces of members are zero, and therefore the axial stiffness of the X-joints is only related to geometric parameters. Then formulae of the parameters, η_{N0}, ω_{N95}, ω_{N50}, and ω_{N10} can be expressed as (Qiu and Zhao, 2009)

$$\eta_{N0}=\psi_{\eta}^{\sigma/f_y}\psi_{\eta}^{\sigma_1/f}\psi_{\eta}^{\sigma_W/f}\psi_{\eta}^{\beta_2}f_{\eta}(\beta,\gamma,\tau,\theta), \quad (3)$$

$$\omega_{N95}=\psi_{N95}^{\sigma/f_y}\psi_{N95}^{\sigma_1/f}\psi_{N95}^{\sigma_W/f}\psi_{N95}^{\beta_2}f_{N95}(\beta,\gamma,\tau,\theta), \quad (4)$$

$$\omega_{N50}=\psi_{N50}^{\sigma/f_y}\psi_{N50}^{\sigma_1/f}\psi_{N50}^{\sigma_W/f}\psi_{N50}^{\beta_2}f_{N50}(\beta,\gamma,\tau,\theta), \quad (5)$$

$$\omega_{N10}=\psi_{N10}^{\sigma/f_y}\psi_{N10}^{\sigma_1/f}\psi_{N10}^{\sigma_W/f}\psi_{N10}^{\beta_2}f_{N10}(\beta,\gamma,\tau,\theta), \quad (6)$$

where ψ^{σ/f_y}, $\psi^{\sigma_1/f}$, $\psi^{\sigma_W/f}$, and ψ^{β_2} are influence coefficients of σ/f_y, M_I, M_W, and β_2, respectively.

The regression sequence is as follows: the function of the geometric parameters $f(\beta, \gamma, \tau, \theta)$ is analyzed first, and then the coefficients relating to the internal force of the joints ψ^{σ/f_y}, $\psi^{\sigma_1/f}$, $\psi^{\sigma_W/f}$, and ψ^{β_2} are obtained. Consequently, η_{N0}, ω_{N95}, ω_{N50}, and ω_{N10} can be determined by Eqs. (3)–(6). Parameter ω_N can be calculated by Eq. (1), and η_N can be evaluated from the curve shown in Fig. 15. Finally, the joint axial stiffness K_N can be obtained by Eq. (2).

6.1 Parametric equations

Firstly, the regression is carried out for η_{N0} on the basis of the geometric parameters, β, γ, τ, and θ. The axial stiffness of those joints, which are closer to the connected brace (e.g., $\eta_{N0}\approx1$), has a more significant effect on the behavior of tubular structures. On the other hand, when η_{N0} is large enough (e.g., $\eta_{N0}>10$), the non-rigidity behavior of CHS X-joints can be ignored. Thus, the data of $\eta_{N0}>10$ are not included in the regression process to ensure the precision of regression. Functions of the other variables, including σ/f_y, M_I, M_W, and β_2, are regressed. Finally the formula for η_{N0} is obtained as

$$\eta_{N0}=29.144\psi_{\eta}^{\sigma/f_y}\psi_{\eta}^{\sigma_1/f}\psi_{\eta}^{\sigma_W/f}\psi_{\eta}^{\beta_2}\times\beta^{0.499}(1-\beta)^{-0.948}\gamma^{-1.448}\tau^{-0.945}(\sin\theta)^{-2.463}, \quad (7)$$

where

$$\psi_{\eta}^{\sigma/f_y}=1.0,\ \psi_{\eta}^{\sigma_1/f}=1.0,$$

$$\psi_{\eta}^{\sigma_W/f}=\frac{1.0}{1.0-0.0263\sigma_W/f+1.016(\sigma_W/f)^3},$$

$$\psi_{\eta}^{\beta_2}=\left(\frac{\beta_2}{\beta}\right)^{0.308}\left(\frac{1-\beta_2}{1-\beta}\right)^{-0.144},\ \beta=0.9 \text{ when } \beta>0.9.$$

The equations of ω_{N95}, ω_{N50}, and ω_{N10}, obtained by the same regression methods, are given as

$$\omega_{N95}=0.282\psi_{N95}^{\sigma/f_y}\psi_{N95}^{\sigma_1/f}\psi_{N95}^{\sigma_W/f}\psi_{N95}^{\beta_2}\times\beta^{0.203}(1-\beta)^{0.028}\gamma^{0.078}\tau^{-0.219}(\sin\theta)^{-0.886}, \quad (8)$$

$$\omega_{N50}=0.286\psi_{N50}^{\sigma/f_y}\psi_{N50}^{\sigma_1/f}\psi_{N50}^{\sigma_W/f}\psi_{N50}^{\beta_2}\times\beta^{0.185}(1-\beta)^{0.197}\gamma^{0.492}\tau^{0.154}(\sin\theta)^{-0.134}, \quad (9)$$

$$\omega_{N10}=0.525\psi_{N10}^{\sigma/f_y}\psi_{N10}^{\sigma_1/f}\psi_{N10}^{\sigma_W/f}\psi_{N10}^{\beta_2}\times\beta^{0.292}(1-\beta)^{0.265}\gamma^{0.533}\tau^{0.227}(\sin\theta)^{0.318}, \quad (10)$$

where

$$\psi_{N95}^{\sigma/f_y}=1-0.406\sigma/f_y-0.325(\sigma/f_y)^2+0.354(\sigma/f_y)^3,$$

$$\psi_{\mathrm{N95}}^{\sigma_1/f}=1.00064/(1+0.00064\mathrm{e}^{8.167(\sigma_1/f)}),$$

$$\psi_{\mathrm{N95}}^{\sigma_\mathrm{w}/f}=1.0+1.706\sigma_\mathrm{w}/f-6.649(\sigma_\mathrm{w}/f)^2+5.964(\sigma_\mathrm{w}/f)^3,$$

$$\psi_{\mathrm{N95}}^{\beta_2}=\left(\frac{\beta_2}{\beta}\right)^{-0.00908}\left(\frac{1-\beta_2}{1-\beta}\right)^{0.143},\ \beta=0.9 \text{ when } \beta>0.9,$$

$$\psi_{\mathrm{N50}}^{\sigma/f_\mathrm{y}}=1-0.107\sigma/f_\mathrm{y}-0.447(\sigma/f_\mathrm{y})^2+0.098(\sigma/f_\mathrm{y})^3,$$

$$\psi_{\mathrm{N50}}^{\sigma_1/f}=1.0129/(1+0.0129\mathrm{e}^{2.852(\sigma_1/f)}),$$

$$\psi_{\mathrm{N50}}^{\sigma_\mathrm{w}/f}=1.0-0.394\sigma_\mathrm{w}/f+1.309(\sigma_\mathrm{w}/f)^2-0.492(\sigma_\mathrm{w}/f)^3,$$

$$\psi_{\mathrm{N50}}^{\beta_2}=\left(\frac{\beta_2}{\beta}\right)^{-0.244}\left(\frac{1-\beta_2}{1-\beta}\right)^{-0.00136},\ \beta=0.9 \text{ when } \beta>0.9,$$

$$\psi_{\mathrm{N10}}^{\sigma/f_\mathrm{y}}=1-0.033\sigma/f_\mathrm{y}-0.304(\sigma/f_\mathrm{y})^2+0.031(\sigma/f_\mathrm{y})^3,$$

$$\psi_{\mathrm{N10}}^{\sigma_1/f}=1.0,$$

$$\psi_{\mathrm{N10}}^{\sigma_\mathrm{w}/f}=1.0-0.574\sigma_\mathrm{w}/f+2.156(\sigma_\mathrm{w}/f)^2-1.339(\sigma_\mathrm{w}/f)^3,$$

$$\psi_{\mathrm{N10}}^{\beta_2}=\left(\frac{\beta_2}{\beta}\right)^{-0.262}\left(\frac{1-\beta_2}{1-\beta}\right)^{0.0391},\ \beta=0.9 \text{ when } \beta>0.9.$$

Then the coefficients a, b, c, and s can be calculated by

$$b=\frac{0.45\omega_{\mathrm{N10}}^2+0.4\omega_{\mathrm{N95}}^2-0.85\omega_{\mathrm{N50}}^2}{(\omega_{\mathrm{N50}}-\omega_{\mathrm{N10}})(\omega_{\mathrm{N95}}-\omega_{\mathrm{N50}})(\omega_{\mathrm{N95}}-\omega_{\mathrm{N10}})}\eta_{\mathrm{N0}}, \quad (11)$$

$$c=\frac{0.85\omega_{\mathrm{N50}}-0.45\omega_{\mathrm{N10}}-0.4\omega_{\mathrm{N95}}}{(\omega_{\mathrm{N50}}-\omega_{\mathrm{N10}})(\omega_{\mathrm{N95}}-\omega_{\mathrm{N50}})(\omega_{\mathrm{N95}}-\omega_{\mathrm{N10}})}\eta_{\mathrm{N0}}, \quad (12)$$

$$a=0.1\eta_{\mathrm{N0}}-b\omega_{\mathrm{N10}}-c\omega_{\mathrm{N10}}^2, \quad (13)$$

$$s=b+2c\omega_{\mathrm{N95}}. \quad (14)$$

The parameter s is the slope at point B of the quadratic curve, BCD, shown in Fig. 15. When $s\leq 0$, section BCD can be simulated as a quadratic curve and functions between η_N and ω_N are shown:

$$\eta_\mathrm{N}=\begin{cases}\left(1-0.05\dfrac{\omega_\mathrm{N}}{\omega_{\mathrm{N95}}}\right)\eta_{\mathrm{N0}}, & \omega_\mathrm{N}\leq\omega_{\mathrm{N95}},\\ a+b\omega_\mathrm{N}+c\omega_\mathrm{N}^2, & \omega_{\mathrm{N95}}<\omega_\mathrm{N}<\omega_{\mathrm{N10}}.\end{cases} \quad (15)$$

When $s>0$, this section cannot be simulated as a quadratic curve, but rather a bilinear curve, and η_N is calculated by

$$\eta_\mathrm{N}=\begin{cases}\left(1-0.05\dfrac{\omega_\mathrm{N}}{\omega_{\mathrm{N95}}}\right)\eta_{\mathrm{N0}}, & \omega_\mathrm{N}\leq\omega_{\mathrm{N95}},\\ \left(0.5+\dfrac{0.45(\omega_\mathrm{N}-\omega_{\mathrm{N50}})}{(\omega_{\mathrm{N95}}-\omega_{\mathrm{N50}})}\right)\eta_{\mathrm{N0}}, & \omega_{\mathrm{N95}}<\omega_\mathrm{N}\leq\omega_{\mathrm{N50}},\\ \left(0.1+\dfrac{0.4(\omega_\mathrm{N}-\omega_{\mathrm{N10}})}{(\omega_{\mathrm{N50}}-\omega_{\mathrm{N10}})}\right)\eta_{\mathrm{N0}}, & \omega_{\mathrm{N10}}<\omega_\mathrm{N}<\omega_{\mathrm{N50}}.\end{cases} \quad (16)$$

6.2 Comparison with finite element results

The axial stiffness of the CHS X-joints under brace axial tension has been predicted by the proposed equations, and the predictions compare reasonably well with the current FE results. The normal distribution of the resulting histogram of predicted axial stiffness to current FE data ratio is shown in Fig. 16. The mean value of 863 data points is 0.97 and the standard deviation is 0.155, indicating that the proposed Eqs. (15) and (16) can provide a consistent prediction of the axial stiffness of CHS X-joints under brace axial tension.

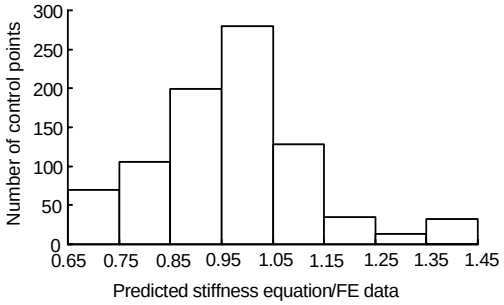

Fig. 16 Predicted axial stiffness to FE data ratio

7 Conclusions

A parametric study of the factors influencing the axial stiffness of CHS X-joints subjected to brace tension has been presented. Single-parameter analyses, covering related factors and considering geometrical and material nonlinearities, have been implemented by the FE package, ANSYS. Based on the FE results of the parametric study, formulae for calculating the axial stiffness of CHS X-joints subjected to brace tension are proposed using the multivariate regression method. The proposed formulae can provide an estimation of the axial stiffness for CHS

X-joints under brace tension in steel tubular structural design.

Two intermediate parameters are introduced to regress the axial stiffness formulae for CHS X-joints under brace tension. The discretized η_N-ω_N curves reflect the relationship between the brace axial tension and the axial stiffness of X-joints. Functions between the two factors are also derived by the multivariate regression technique.

The joint stiffness under brace tension decreases with increases in brace axial load, especially when the axial load is large. The joint axial stiffness increases with increases in β, but decreases with increases in γ and θ. The parameter τ has a minor effect on the joint stiffness. The effect of the other brace diameter must be considered when the two brace diameters are different.

References

Chen, T.Y., Zhang, H.Y., 1996. Stress analysis of spatial frames with consideration of local flexibility of multiplanar tubular joint. *Engineering Structures*, **18**(6):465-471. [doi:10.1016/0141-0296(95)00109-3]

Chen, Y.Y., Wang, W., Zhao, X.Z., Jiang, X.Y., Bai, X., Zhao, Z.Y., 2001. Experiments on bending rigidity and resistance of unstiffened tubular joints. *Journal of Building Structures*, **22**(6):25-30 (in Chinese).

Choo, Y.S., Qian, X.D., Liew, J.Y.R., Wardenier, J., 2003. Static strength of thick-walled CHS X-joints. Part II. Effect of chord stresses. *Journal of Constructional Steel Research*, **59**(10):1229-1250. [doi:10.1016/S0143-974X(03)00053-1]

Choo, Y.S., Qian, X.D., Wardenier, J., 2006. Effects of boundary conditions and chord stresses on static strength of thick-walled CHS K-joints. *Journal of Constructional Steel Research*, **62**(4):316-328. [doi:10.1016/j.jcsr.2005.08.001]

GB 50017-2003. Code for Design of Steel Structures. Chinese Standard. Chinese Plan Press, Beijing, China (in Chinese).

Gho, W.M., Yang, Y., 2008. Parametric equation for static strength of tubular circular hollow section joints with complete overlap of braces. *Journal of Structural Engineering*, **134**(3):393-401. [doi:10.1061/(ASCE)0733-9445(2008)134:3(393)]

Gho, W.M., Yang, Y., Gao, F., 2006. Failure mechanisms of tubular CHS joints with complete overlap of braces. *Thin-Walled Structures*, **44**(6):655-666. [doi:10.1016/j.tws.2006.05.007]

Ihaddoudenea, A.N.T., Saidani, M., Chemrouka, M., 2009. Mechanical model for the analysis of steel frames with semi rigid joints. *Journal of Constructional Steel Research*, **65**(3):631-640. [doi:10.1016/j.jcsr.2008.08.010]

Lopez, A., Puente, I., Serna, M.A., 2007. Numerical model and experimental tests on single-layer latticed domes with semi-rigid joints. *Computers and Structures*, **85**(7-8):360-374. [doi:10.1016/j.compstruc.2006.11.025]

Qian, X., Dodds, R.H., Choo, Y.S., 2005. Elastic-plastic crack driving force for tubular X-joints with mismatched welds. *Engineering Structures*, **27**(9):1419-1434. [doi:10.1016/j.engstruct.2005.03.013]

Qiu, G.Z., Zhao, J.C., 2008. Experimental research on rigidity of circular tubular X-joints. *Journal of Shanghai Jiaotong University*, **42**(6):966-970 (in Chinese).

Qiu, G.Z., Zhao, J.C., 2009. Analysis and calculation of axial stiffness of tubular X-joints under compression on braces. *Journal of Shanghai Jiaotong University (Science)*, **14**(4):410-417. [doi:10.1007/s12204-009-0410-y]

Qiu, G.Z., Zhao, J.C., 2010. Influence of joint stiffness on stability behavior of a single-layer reticulated shell. *Building Structure*, **40**(3):97-99, 117 (in Chinese).

SAS, 2002. ANSYS User's Manual, Revision 6.1. Swanson Analysis Systems, Inc., PA, USA.

Schumacher, A., Borges, L.C., Nussbaumer, A., 2009. A critical examination of the size effect correction for welded steel tubular joints. *International Journal of Fatigue*, **31**(8-9):1422-1433. [doi:10.1016/j.ijfatigue.2009.04.003]

Shu, X.P., Zhu, S.N., Xia, X.H., Yang, X., 2004. Full-scale experiment research on CHS joints of steel roof of He Long Stadium in Changsha. *Journal of Building Structures*, **25**(3):11-13 (in Chinese).

Soh, C.K., Chan, T.K., Yu, S.K., 2000. Limit analysis of ultimate strength of tubular X-joints. *Journal of Structural Engineering*, **126**(7):790-797. [doi:10.1061/(ASCE)0733-9445(2000)126:7(790)]

Turker, T., Kartal, M.E., Bayraktar, A., 2009. Assessment of semi-rigid connections in steel structures by modal testing. *Journal of Constructional Steel Research*, **65**(7):1538-1547. [doi:10.1016/j.jcsr.2009.03.002]

Wang, W., 2005. Non-Rigid Behavior of Unstiffened Circular Tubular Joints and Their Effects on Global Performance of Steel Tubular Structures. PhD Thesis, Tongji University, Shanghai, China (in Chinese).

Wang, W., Chen, Y.Y., 2005. Modeling and classification of tubular joint rigidity and its effect on the global response of CHS lattice girders. *Journal of Structural Engineering and Mechanics*, **21**(6):677-698.

Yang, L.X., Chen, T.Y., Wu, S.Y., 1990. Local flexibility behavior of tubular joints and its effect on global analysis of tubular structures. *China Ocean Engineering*, **4**(4):371-384.